AD-A069 711 HUGHES RESEARCH LABS MALIBU CALIF F/G 20/6
GEODESIC LENSES FOR INTEGRATED OPTIC CIRCUITS.(U)
MAY 79 B CHEN, O G RAMER N00173-78-C-0102
UNCLASSIFIED NL

1 OF 1
AD A069711

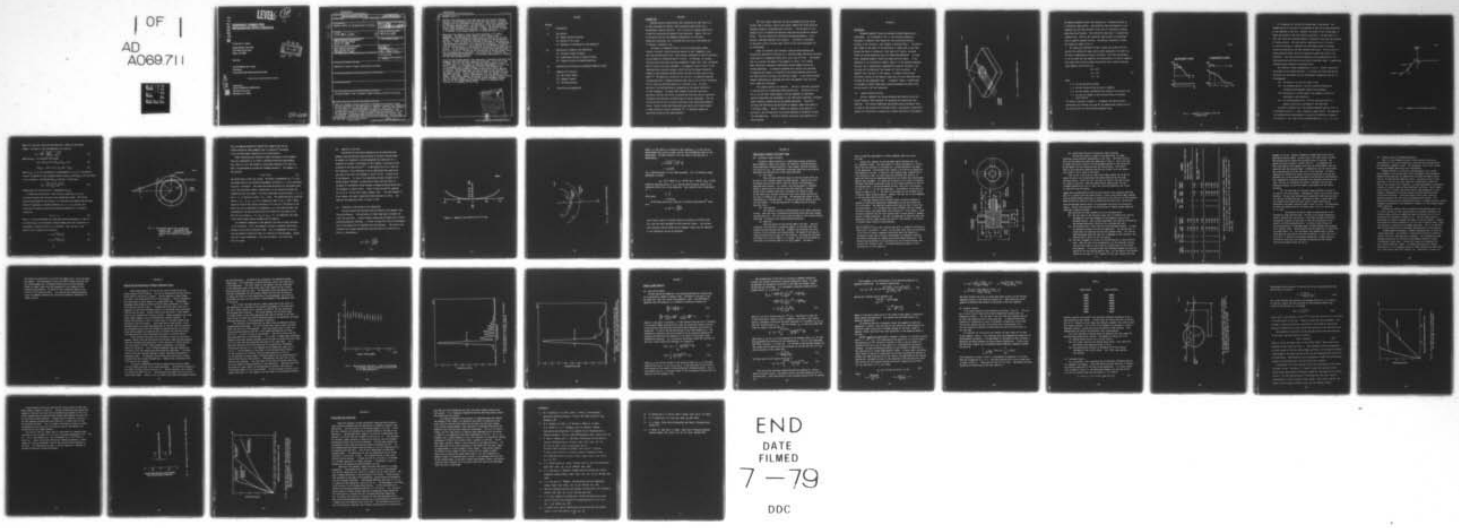

END
DATE FILMED
7-79
DDC

LEVEL II (12)

3

GEODESIC LENSES FOR INTEGRATED OPTIC CIRCUITS

B. Chen and O. G. Ramer

Hughes Research Laboratories
3011 Malibu Canyon Road
Malibu, CA 90265

May 1979

Contract N00173–78–C–0102
Final Report
For period 25 April 1978 through 24 April 1979

Approved for public release; distribution unlimited.

Sponsored by
NAVAL RESEARCH LABORATORY
455 Overlook Ave. S.W.
Washington, D.C. 20375

UNCLASSIFIED

SECURITY CLASSIFICATION OF THIS PAGE (When Data Entered)

REPORT DOCUMENTATION PAGE	READ INSTRUCTIONS BEFORE COMPLETING FORM
1. REPORT NUMBER	2. GOVT ACCESSION NO. / 3. RECIPIENT'S CATALOG NUMBER
4. TITLE (and Subtitle): Geodesic Lenses for Integrated Optic Circuits,	5. TYPE OF REPORT & PERIOD COVERED: Final Report, 25 Apr 78-24 Apr 79
7. AUTHOR(s): B. Chen & G. G. Ramer	8. CONTRACT OR GRANT NUMBER(s): N00173-78-C-0102
9. PERFORMING ORGANIZATION NAME AND ADDRESS: Hughes Research Laboratories, 3011 Malibu Canyon Road, Malibu, CA 90265	10. PROGRAM ELEMENT, PROJECT, TASK AREA & WORK UNIT NUMBERS
11. CONTROLLING OFFICE NAME AND ADDRESS: Naval Research Laboratory, 4555 Overlook Ave. S.W., Washington, D.C. 20375	12. REPORT DATE: May 1979 / 13. NUMBER OF PAGES: 43 (12) 47p.
14. MONITORING AGENCY NAME & ADDRESS(if different from Controlling Office)	15. SECURITY CLASS. (of this report): Unclassified / 15a. DECLASSIFICATION/DOWNGRADING SCHEDULE

16. DISTRIBUTION STATEMENT (of this Report)

Approved for public release; distribution unlimited

17. DISTRIBUTION STATEMENT (of the abstract entered in Block 20, if different from Report)

18. SUPPLEMENTARY NOTES

19. KEY WORDS (Continue on reverse side if necessary and identify by block number)

Waveguide geodesic lens, ultrasonic impact grinding, optical ray tracing

20. ABSTRACT (Continue on reverse side if necessary and identify by block number)

Under this program, we have successfully developed the ultrasonic impact grinding technique for the fabrication of aspherical geodesic lens depressions. The lens radius is 4 mm and the depth is 1.374 mm. 15% of the lens aperture is allocated for a curved rounding at the edge of the depression. The designed focal length is 10.2 mm for an aberration free aperture of 6.8 mm. The technique of ultrasonic impact grinding is proved to be precise, fast and economic. Reproducible results can be easily obtained. The tool wear

DD FORM 1 JAN 73 1473 EDITION OF 1 NOV 65 IS OBSOLETE
S/N 0102-LF-014-6601

172 600

SECURITY CLASSIFICATION OF THIS PAGE (When Data Entered)

micrometers

20. ABSTRACT (cont'd.)

problem can be neglected if more than two tools are used for grinding the lens. We have demonstrated that depth variation within 7.5 μm for 5 depressions can be obtained using two tools. One of the 5 depressions has the exact designed depth. The consistency of the lens depressions can be further improved if a third tool is used. The grinding process is fast using the 200 W Bullen machine. It takes only 45 sec. to grind a 1.4 mm deep, 8 mm diameter depression in $LiNbO_3$ substrate.

Aberration free geodesic lenses have been fabricated in Ti:$LiNbO_3$ waveguides. The measured focal length is fairly close to the designed 10.2 mm even though the lens profile is slightly off the ideal profile. The major fabrication problem encountered is the polishing of the lenses. There are many fine scratches at the edge of the depression, causing excessive propagation loss and in-plane scattering. The measured 3 dB focal spot size is 1.6 μm as compared to the theoretical value of 0.32 μm. The discrepancy is believed to be the sum of the following three effects. (1) The resolution of a perfect 10x microscope objective with NA = 0.3 is 0.93 μm. (2) The use of prism coupler to extract guided light out of waveguide causes aberration. The rutile prism is uniaxial and introduces additional aberration. (3) The actual lens profile is slightly off the ideal designed profile.

A ray tracing through geodesic lens depression is developed from which the geometric spot size and focal length are calculated. For an f/1.5 lens in $LiNbO_3$, the full lobe width of a Gaussian beam truncated at the 1/e points is about 1.4 μm assuming the free space wavelength is 0.8 μm. For a 1 cm diameter lens, a depth change of 1% can still maintain its diffraction limited performance if 90% of the original useful aperture is utilized. On the other hand, the focal length is very sensitive to the depth variation. We have shown that for each unit decrease in total depth for tool wear, there is approximately a 13 unit change in focal length. With surface removal, the change in focal length is about 3 units per unit change in depth. Unless one can control the depth to better than 1.0 μm, the integration of geodesic lenses in integrated optic circuits is an extremely difficult job.

OUTLINE

SECTION

I Introduction

II Lens Design

(a) General Design Principles

(b) Design of F/1.5 Lens

(c) Radiation at the Bottom of Lens Depression

III Fabrication of Geodesic Lens Depression

(a) Ultrasonic Impact Grinding

(b) Experimental Results of Impact Grinding

(c) Diamond Turning and Diamond Generating

IV Fabrication and Evaluation of Waveguide Geodesic Lenses

V Computer Error Analysis

(a) Ray Tracing Theory

(b) Computer Program

(c) Tolerance Analysis

VI Conclusions and Suggestions

SECTION I

INTRODUCTION

Coherent optical processing has been considered for some time to be an ideal technique for several signal-processing applications (e.g., correlations, spectral analysis). This is due to its unique capabilities of parallel processing and speed-of-light operation. However, the size of the device and its environmental vulnerability (to vibration, temperature variations, etc.) precluded the field use of the method and it remained a laboratory tool.

The advent of integrated optical circuits has generated renewed interest in optical signal processing because of their ruggedness, small size, and low fabrication cost. Most previous objections to optical processors can be removed by integrated optical circuits. In addition, for systems requiring fast processing large data bandwidths (larger than 1 GHz), integrated optical circuits are prime contenders. An example of such a circuit is the integrated optic spectrum analyzer, which utilizes the Bragg interaction between a surface-guided coherent optical wave and a surface acoustic wave (SAW).[1,2] The operating principle of the circuit is to spatially modulate a guided beam with a frequency-modulated SAW, then to use a Fourier transform lens to focus the deflected beam on to a detector array. The focal position of the deflected beam is determined by the angular deflection (or SAW frequency). To obtain high frequency resolution from these operations requires the ability to perform the two basic optical operations, collimation and focusing, on guided beams in optical waveguides. Both are limited by the ability to construct aberration-free single mode waveguide lenses. Several recent published papers have dealt with various aspects of beam focusing in optical waveguides.[3-8] In addition, methods of aberration correction have been proposed.[3]

This final report summarizes the work performed during the period 25 April 1978 to 24 April 1979 on the contract (N00173-78-C-0102) entitled "Geodesic Lenses for Integrated Optic Circuits". The key goals of this program are (a) to develop and fabricate high precision aspherical geodesic lenses. The lens should have diffraction-limited performance; (b) to perform a simulated computer error analysis. The effect of deviation of the actual profile from the ideal profile on the lens performance will be investigated.

Under this program, the ultrasonic impact grinding technique was successfully developed to fabricate in Ti diffused $LiNbO_3$ aberration corrected, single mode f/1.5 waveguide lenses with a focal lens of 10 mm. The program goal is to control the depth of the geodesic to within 1 μm or better. Other fabrication techniques investigated include diamond turning and diamond generating. An extensive computer error analysis was performed to determine the effects of deviation of the actual machined profile from the ideal profile on the spot size and focal length. A ray tracing through geodesic depression was developed from which the geometric spot size and focal length are calculated.

This report consists of 5 sections. Section II discusses the design of lens profile for an aberration-free focusing lens. The profile for an f/1.5, 10.2 mm focal length geodesic lens was computed for experiment. Section III describes the development of lens fabrication techniques, ultrasonic impact grinding, diamond turning and diamond generating. Section IV discusses the fabrication and evaluation of geodesic lenses fabricated in Ti diffused $LiNbO_3$. Section V reports the computer error analysis, in particular, the utilization of ray tracing technique to determine the spot size and aberration. Section VI reports conclusions and suggestions for future studies.

SECTION II

LENS DESIGN

Waveguide geodesic lenses are waveguide-covered depressions or protrusions. As illustrated in Fig. 1, the curvature generates a difference in geometric path length for rays traversing different portions of the structure; this produces a focusing effect. The optical path length at the center of the depression is longer than at the sides. Because the index of refraction is the same at all points, the phase fronts are curved toward the lens axis beyond the depression. In other words, waveguide geodesic lenses are always positive lenses. If the depression is of a particular aspheric shape or if the wavefront emerging from the line is appropriately compensated by external overlayers, the focusing will be aberration free (except for field curvature). The aspheric lens, the topic of this report, is formed by grinding and polishing a surface to the aspheric shape that will give aberration-free focusing for the waveguided light. In geodesic lenses, a rounded edge is included to prevent undesirable scattering between the planar guide and the guide in the lens depression.

(a) General Design Principle

We use a geodesic lens design procedure described by Kassai and Marom;[9] however, their procedure for designing the rounding has been modified. This section summarizes the modified design procedure, which is based on the principle of equivalent lenses, and presents a generalized method for calculating a rounding with a smooth transition to the geodesic.

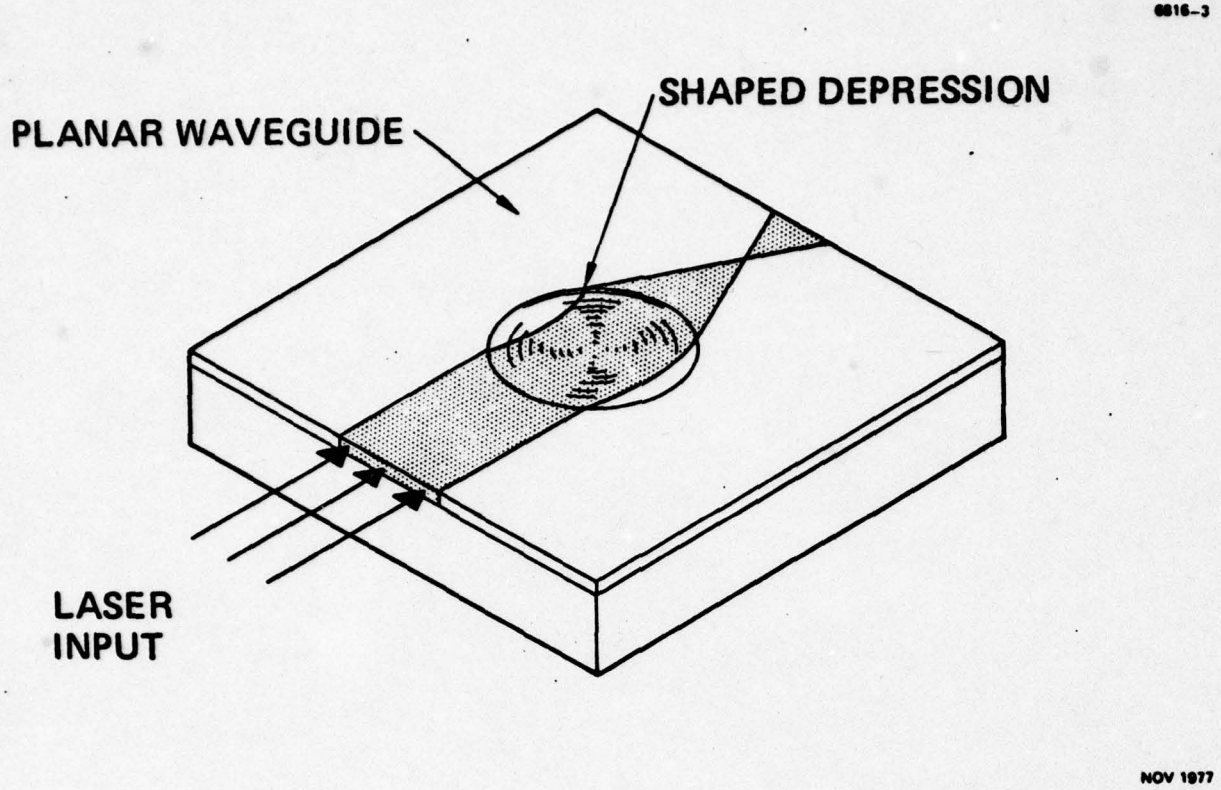

Fig. 1 Configuration of Geodesic Lens

The design procedure entails the conversion of a rounding function to a refractive index profile. The refractive index distribution in the remainder (or the inner portion) of the lens is calculated to achieve aberration-free focusing. This refractive index lens is a generalized Luneberg lens. Finally, the refractive index profile is transformed into an aspheric geodesic profile. The physical properties of these two lenses are shown in Fig. 2.

Two lenses are equivalent if their indices and surface profiles satisfy the condition of equal optical path length, where the optical or ray path is determined by Fermat's principle. Using this equivalence, it can be shown that the equations for transforming a circularly symmetric flat guide with a refractive index distribution and a uniform refractive index geodesic lens profile are

$$\begin{aligned} n\delta s &= \bar{n}\delta\bar{s} \\ n\rho &= \bar{n}\bar{\rho} \\ \delta\theta &= \delta\bar{\theta} \end{aligned} \tag{1}$$

where

- $n, \bar{n}$ are the refractive indices
- $\rho, \bar{\rho}$ are the distances from the axis of symmetry
- $\theta, \bar{\theta}$ are the angular coordinates with respect to the optical axis
- $s, \bar{s}$ are the arc lengths of the structure along a meridional cross section.

For planar structures, $\bar{\rho}$ equals $\bar{s}$. Throughout this report, barred coordinates and variables are used for the generalized Luneberg profile and unbarred ones for the equivalent geodesic lens.

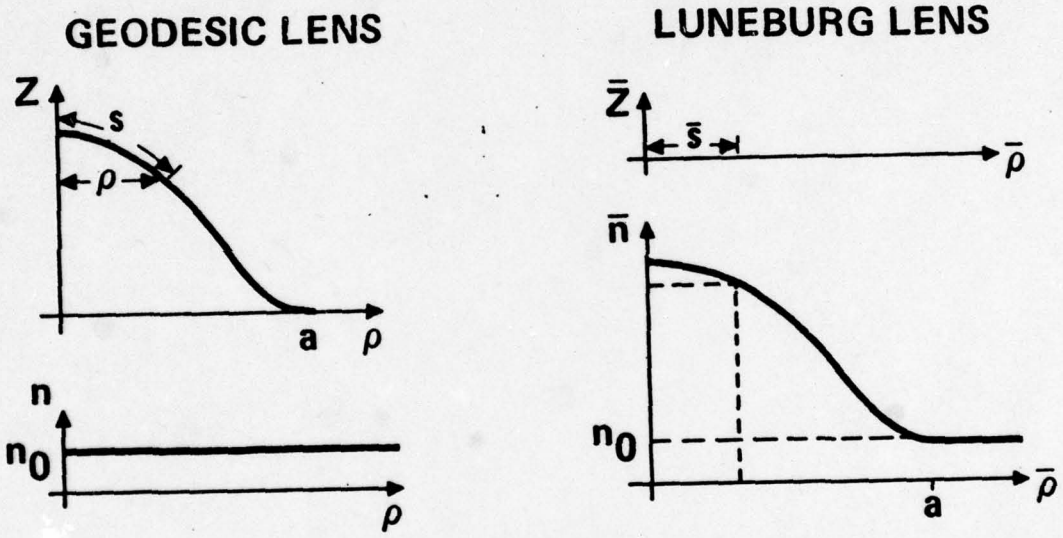

Fig. 2 Parameters of Geodesic Lens and Luneberg Lens

It is necessary to include the rounded edge in the design. The rounded portion of the lens is not expected to have the focusing properties of the remainder of the lens. However, the effect of the rounded edge is taken into account in the lens profile calculation. The end result is a lens that (with the rounding present) is aberration free with the exception of field curvature. The lens profile described in Ref. 9 (in which a circular rounding was used) were not sufficiently smooth to prevent excessive scattering at the lens rounding transitions. This was due to a rapid curvature change, which was necessary to match the slope at the transition. This rapid curvature change was also accompanied by a discontinuous second derivative in the profile functional shape. A generalized rounding design procedure is described below.

The rounding is shown schematically in Fig. 3. Several constraints are placed on the rounding function, r, to reduce the scattering and the insertion loss associated with the disturbance introduced by the lens in the waveguide:

(i) The slope of r at the lens edge is zero

(ii) The rounding function r and the transition between the rounding and the geodesic profile are continuous

(iii) The slope of r and the slope of the geodesic profile are continuous at the transition

(iv) The second derivative of r and the second derivative of geodesic profile are continuous at the transition.

To design a Luneberg lens, the proposed rounding function, r(x), is transformed, using Eq. 1, into a refractive index profile. The algorithm for performing the transformation is carried out digitally by stepping the variable $x = R-\rho$ from 0 to the rounding edge (i.e., $x_{i+1} = x_i + \Delta x$),

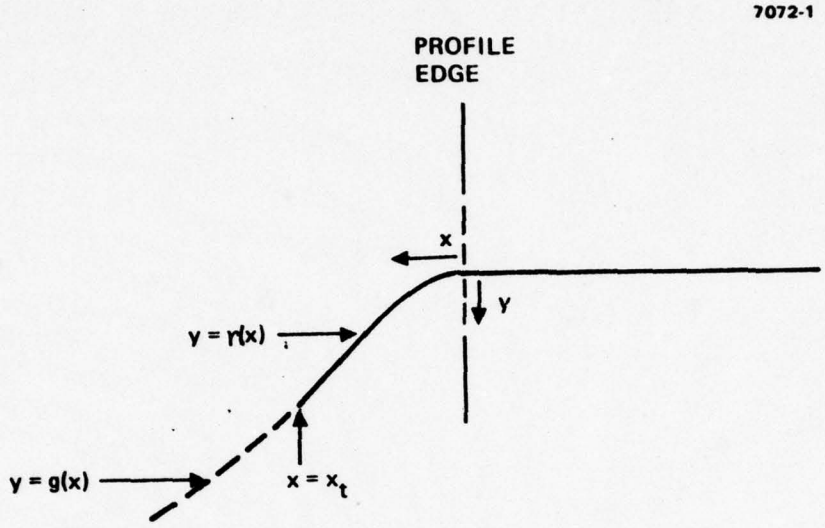

Fig. 3 Schematic of the rounding function

where R is the lens radius and the subscript i refers to the annulus number. For each Δx, the corresponding Δs is given by

$$\Delta s = \Delta x \sqrt{1 + \left(\frac{df}{dx}\Big|_{x_i - \frac{\Delta x}{2}} \right)^2} \tag{2}$$

Rewriting Eq. 1 in different form yields

$$n\Delta s = \bar{n}(\bar{x}_{i+1})\, \Delta\bar{x} = \bar{n}(\bar{x}_{i+1})(\bar{x}_{i+1} - \bar{x}_i) \tag{3}$$

$$\bar{n}(\bar{x}_{i+1}) - n\rho/\bar{\rho} = n(R - \bar{x}_{i+1})/(R - \bar{x}_{i+1}), \tag{4}$$

where $\bar{x}_{i+1} - \bar{x}_i$ is the incremental $\Delta\bar{x}$ corresponding to Δx, $\bar{x}_i$ is the previous value of $\bar{x}$ obtained in the preceding annulus, and $\bar{x}_{i+1}$ and $\bar{n}(\bar{x}_{i+1})$ are the values to be calculated. Eliminating $\bar{n}(\bar{x}_{i+1})$ from Eqs. 3 and 4 gives

$$\bar{x}_{i+1} = \frac{R\Delta s + x_i\,(R - \bar{x}_{i+1})}{R - x_{i+1} + \Delta s}\,. \tag{5}$$

Substituting this result into Eq. 4 determines $\bar{n}(\bar{x}_{i+1})$.

To determine the function r that satisfies conditions (iii) and (iv) above requires the tracing of rays through the system. The initial problem associated with ray tracing is to find which ray coming from the focal point will penetrate a specified distance (i.e., $x = x_t$) into the lens. Light rays are known to satisfy the following condition on a surface of revolution:

$$\rho \sin\alpha = h, \tag{6}$$

where α is the angle between the light path and the meridian at ρ, and h is a constant equal to the shortest distance between the light trajectory on the geodesic surface and the axis of rotation. Thus, for any x, the angles α and ψ (Figure 4) are given by

$$\alpha = \sin^{-1}\left[\frac{R - x}{R}\right] \tag{7}$$

$$\psi = \sin^{-1}\left[\frac{R}{f}\sin\alpha\right] \tag{8}$$

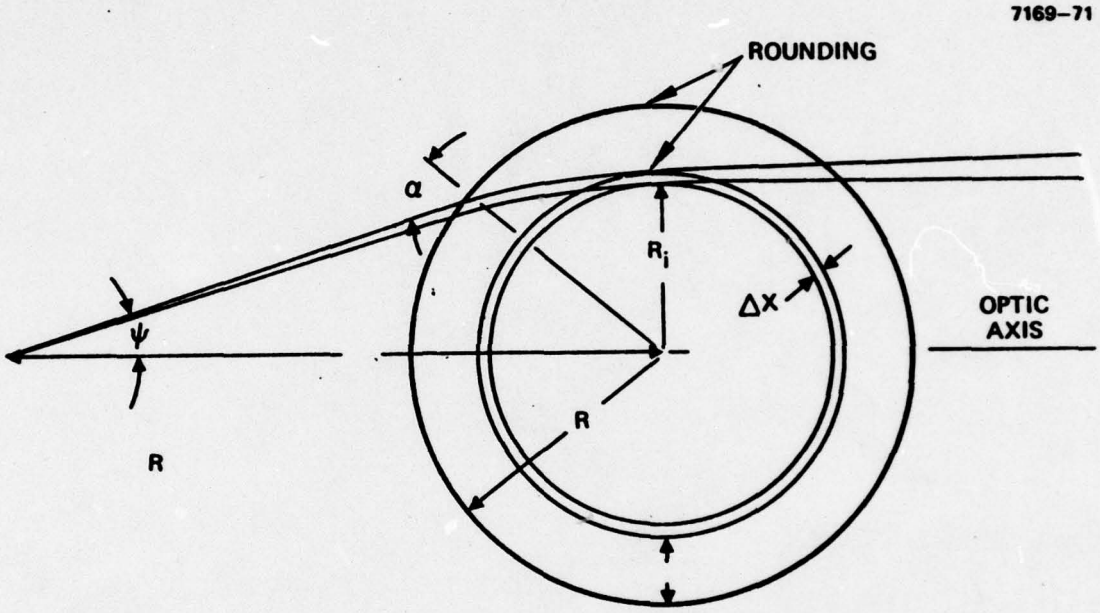

Fig. 4 Ray tracing through the rounded edge geodesic lens. Rays penetrating into the lens, exceeding the rounding annulus, exit parallel to the optic axis.

Since the mapping between the generalized Luneberg lens and the uniform refractive index geodesic lens is conformal,[9] the angles α and ψ are the angles required for ray initialization.

After calculating the refractive index distribution of the Luneberg lens and transforming it to create a constant-refractive-index geodesic lens, there is still the problem of satisfying conditions (iii) and (iv). This is accomplished by varying the rounding function f. For example, in the function

$$r = Ax^2 + Bx^3, \tag{9}$$

the coefficients A and B are varied. The points corresponding to $x \geq x_t$ are calculated based on the focusing requirement; the points $x < x_t$ are calculated using Eqs. 2 through 5. The slope and second derivative are calculated using a two- and three-point method, respectively, at the transition between the rounding and the lens region. The slope calculated using the points $x = x_t - \Delta x$ and $x = x_t$ is required to equal $r'(x_t - \Delta x/2)$. The second derivative using the points $x = x_t - \Delta x$, x_t, $x_t + \Delta x$ is required to equal $r''(x_t)$. After finding values of A and B that satisfy conditions (iii) and (iv), the design of the whole lens can be completed by incrementing x or ψ and requiring that rays originating at the desired focal point exit parallel to the optical axis. Each ray at an angle $\psi_i - \Delta\psi = \psi_{i+1}$ or $x_{i+1} = x_i + \Delta x$ determines the index of the central-most annulus through which it transits.

Two important properties of the geodesic lens have not been discussed in the literature. First, the geodesic lens has no chromatic aberrations because of the uniform refractive index. This is independent of the fact that the material refractive index is a function of the wavelength. Second, the lens is mode independent. This may allow multi- and single-mode optical systems.

(b) Design of f/1/5 lens

The profile of the surface depression for an aberration-free geodesic lens was derived using the design principles outlined above. An analysis of radiation in curved waveguides has shown that it is necessary to include in the design of the rounding a constraint on the curvature of the lens profile.[10] In the design of an f/1.5 lens for this contract, it was necessary to use an aberration-free aperture of only 85% of the total lens diameter to avoid cut-off at every point on the geodesic. In view of this experience we have included in our design program "DILIGENT" an algorithm to check that the radius of curvature of the geodesic always exceeds a minimum curvature below which the waveguide is beyond cutoff. Figure 5 shows the profile computed for an f/1.5, 10.2 mm focal length, geodesic lens. The lens diameter is 8 mm, however, the useful (aberration-free) aperture is 6.8 mm. The depth at the depression center is about 1.37 mm.

(c) Radiation at the bottom of lens depression

We have studied the radiation from the bottom of the geodesic lens into the substrate. The derivation of fiber leaky waves by Snyder and Love[11] was used here. Figure 6 shows a guided wave incident onto a curved waveguide-substrate interface. In order to match the field at the boundary part of the energy will be radiated into the substrate. The field in the substrate first decays exponentially and then starts to oscillate at a point x_t, determined by

$$x_t = \frac{\rho}{2}\left(1 - \frac{\sin^2\theta_c}{\sin^2\theta}\right)$$

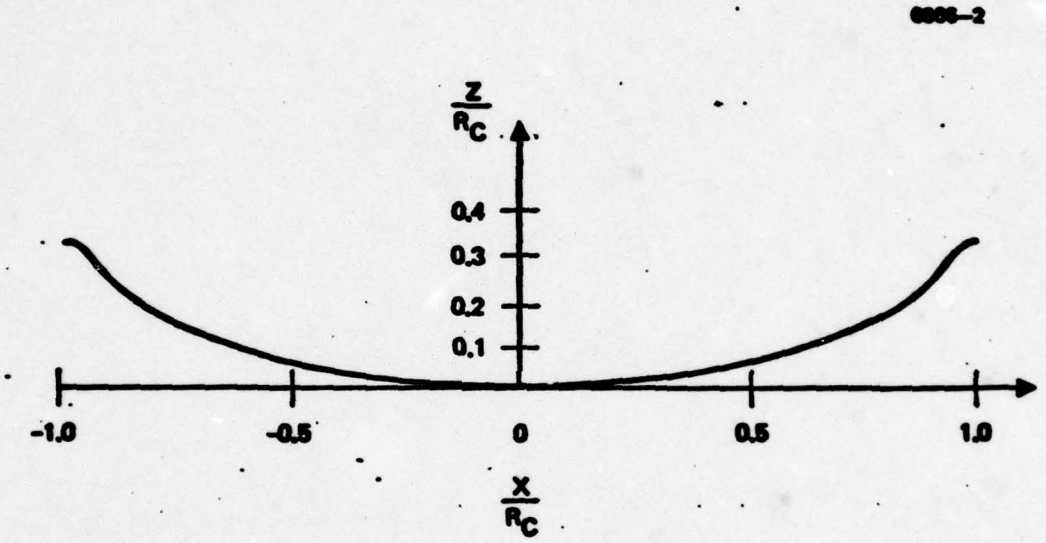

Figure 5. Geodesic lens profile for f/1.5 lens

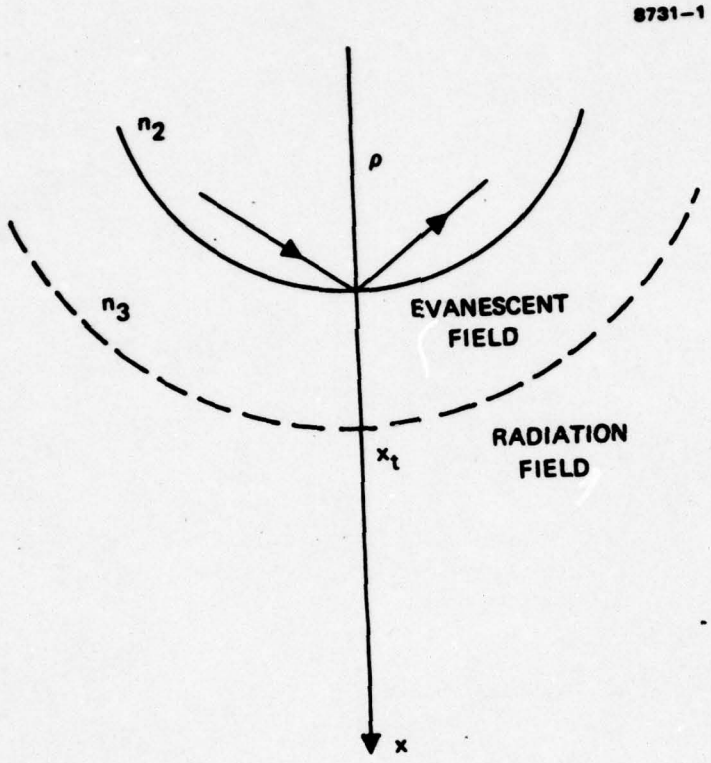

Fig. 6 Reflection at a curved interface

where ρ is the radius of curvature of the interface, θ_c is the critical angle between the n_2 and n_3 media, and θ is the corresponding angle of the guided mode. The decay constant α for the field in the substrate is approximately

$$\alpha = \sqrt{2.205^2 - 2.20^2}\ \frac{2\pi}{\lambda}$$

$$= 0.148\ \frac{2\pi}{\lambda}$$

for a simplified model of step index waveguide. For a Ti-diffused $LiNbO_3$ waveguide, we obtain

$$x_t = \frac{\rho}{2} \times 0.0043 \text{ for } \theta_c = 84.55° \text{ and } \theta = 86.05° \ (n_{eff} \sim 2.205) .$$

Excessive radiation occurs if x_t is smaller than the decay length of the evanescent field ($1/\alpha$) in the substrate. Thus radiation loss is negligible if

$$x_t > \frac{1}{\alpha}$$

which means

$$\rho > 0.44 \text{ mm}$$

An alternate derivation, based on a different approximation,[12] finds that

$$x_t = \frac{\rho}{2}\ (1 - \frac{\sin\theta_c}{\sin\theta})$$

which finally leads to a minimal radius of curvature of 0.88 mm, much less than the radius designed for most practical lenses. We conclude that radiation from the bottom of our geodesic lenses into the substrate is not substantial and can be neglected.

SECTION III

FABRICATION OF GEODESIC LENS DEPRESSIONS

(a) Ultrasonic Impact Grinding

Ultrasonic impact grinding is a complicated process governed by many parameters; namely, tool shape, tool material, grinding pressure, stroke amplitude, workpiece material, slurry speed, abrasive concentration and grit size. The operational conditions under which the grinding experiment was performed are briefly described below.

(1) Tool shape

There are many different shapes of the tool holder which can be used in the ultrasonic impact grinding machine. Tapered tools with the bottom cross section smaller than the top have the advantage of amplitude amplification. As a result, the cutting speed is increased. However, tapered tools do not have long term stability, a constant tuning of the resonance condition is necessary for precision work. On the other hand, straight cylindrical tools have slower cutting rate but stay in resonance for a long time. The designed tool holder in the experiment has a straight shape. It takes an average 45 minutes to grind an 8 mm diameter, 1.5 mm deep depression in $LiNbO_3$ using 20 μm Al_2O_3 abrasive slurry.

(2) Tool material

Tool material should be selected based on its impact resistance to wear. Good tool wear is obtained with material which has high strength and good ductility. The tool tips we used are made of cold rolled stainless steel 420. The material was annealed before machining.

(3) Abrasives

Abrasive grains are the cutting edge of the tool. They are dispersed, with the help of suspension agents, in the water that flows between the workpiece and the tool. Commonly used abrasives are boron carbide, silicon carbide, and aluminum oxide. We choose 20 μm Al_2O_3 for rough grinding and 9 μm Al_2O_3 for fine grinding. The abrasives are mixed with water at a ratio of about 1:1 in volume. We have also purchased an additional recirculation pump for 3 μm Al_2O_3 powder. The pump is

used to study the improvement of surface roughness when finer grits are used.

During this program, we have designed impact grinding tools for f/1.5 geodesic lenses. The lens radius is 4 mm and the depth is 1.374 mm. 15% of the lens aperture is allocated for a curved rounding at the edge of the depression. The designed focal length is 10.2 mm for an aberration free aperture of 6.8 mm. A survey of local machine shops revealed that a 5 μm tolerance in tool tip, which bears the designed lens profile, is about the limit that an experienced machinist can achieve with conventional machine shop equipment. To reduce the tolerance to less than 5 μm requires different fabrication techniques which are not readily available in most of the machine shops.* We have purchased the tool tips with 5 μm tolerance for the f/1.5, F = 10.2 mm lens experiment. The blueprint of the tool tip design is shown in Fig. 7. The tools are designed for our Raytheon 100 W ultrasonic impact grinding machine. However, the tool tip is also adaptable to the new high precision Bullen machine.

It has been reported that ultrasonic impact grinding technique is capable of fabricating depressions complementary to the tool shape with 1/4 μm tolerance. The operation requires more than one tool to avoid the tool wear effect. It is estimated that three different tools are needed to obtain precise lens depressions with tolerance of 1 μm or better. Using the tools purchased from the local machine shop, we have ground 11 geodesic lenses in $LiNbO_3$ substrates. Two tool tips were used to fabricate each lens depression, one for rough grinding and one for fine grinding. The results of grinding these lenses are now presented.

---

*We are unable to find a local machine shop which is capable of fabricating tools with 1 μm profile tolerance. On the other hand, there are techniques in the field of optical component fabrication where the dimensional tolerances on the order of optical wavelengths are frequently achieved. The optical techniques are diamond turning and diamond generating. The diamond turning machine is very expensive and the turning technique does not work for stainless steel. The diamond generating seems a viable technique and is less expensive.

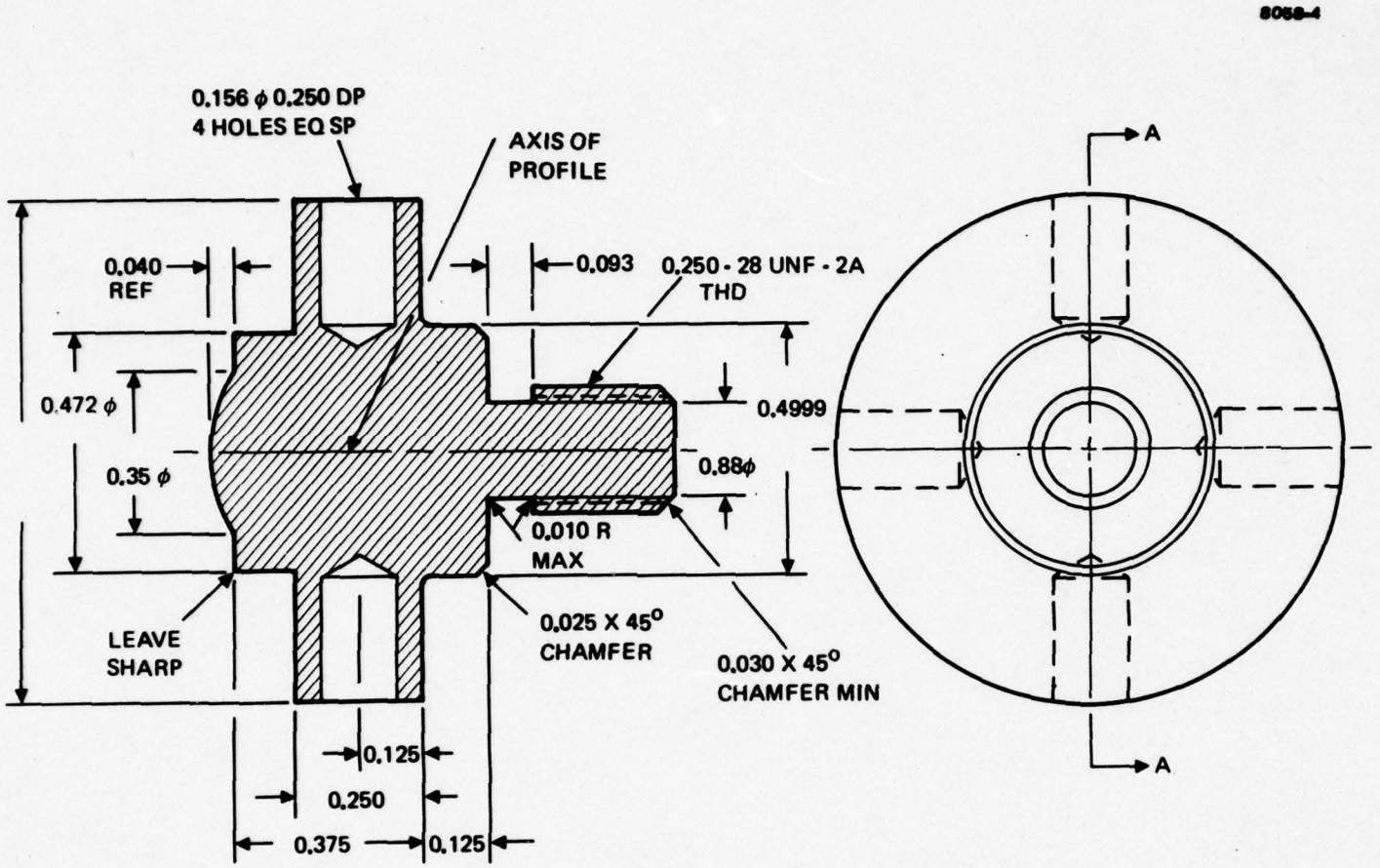

Figure 7. Design of the tool tip for ultrasonic impact grinding

(b) Experimental Results of Ultrasonic Impact Grinding

We have fabricated 11 geodesic lens depressions in $LiNbO_3$ substrates using different combinations of tool tips. The order of using tools and the depression depth are summarized in Table 1. Due to the lack of depth and position control from the Raytheon machine all the lenses are ground deeper into the substrate than the desired depth. The overall depth of each depression measured from the top surface (true lens depth + over grind) is also listed in the Table.

Tool tip No. 2 was used to rough grind $LiNbO_3$ samples 2A, 2B and 2C. Sample 2A had an oval shape because the sample moved during the rough grinding process. After this run, soft wax was used all the time to keep the sample in position. When the sample 2B was rough ground, the tool alignment mechanism was out of order, the resulting depression was tilted at angle more than 10 degrees.

Sample 2C was broken when we tried to tune the tool into resonance while the tool is in contact with the sample surface. After losing three $LiNbO_3$ samples, we have gained enough experience to successfully grind the rest of the 8 samples. Repositioning the sample for fine grinding requires some skill, particularly with the Raytheon machine which is not equipped with precision translation stages. We were very successful in positioning all samples except sample 4B which was slightly misplaced.

The conclusions we have reached so far are discussed below.

(1) The tool wear of the stainless steel tool is slightly less than 2%. The degree of tool wear depends on the parameters used in the grinding process. More careful experiments are required to establish the optimum operational condition for a minimum tool wear.

(2) The grinding rate is fast even with 100 W Raytheon machine. It takes an average 45 minutes to grind the depression. The cutting rate is slower when the contacted working area becomes larger. For the last few thousandths where the tool tip is embedded in the substrate, the cutting rate is about 0.5 mil per minute.

(3) The tool alignment is critical to the fabrication of high precision lens. When the tool is not perpendicular to the substrate surface, the lens thus made will be tilted at an angle equal to the angular misalignment. If we specify that the difference between two opposite points on the lens edge be smaller than 1 μm, the angular misalignment should be less than 7×10^{-3} degree (or 25.8 sec) assuming the lens

$LiNbO_3$ Sample	Rough Grind: Tool No	Rough Grind: Order of Usage	Rough Grind: Lens Depth	Rough Grind: Overall Depth	Fine Grind: Tool No	Fine Grind: Order of Usage	Fine Grind: Lens Depth	Fine Grind: Overall Depth	Comments
2A	2	1	-	-					Oval, sample moved in rough grind
2B	2	2	1.719	1.862					Angular misaligned
2C	2	3	1.693	1.749	1	4			Broken in fine grind
4A	4	1	1.758	2.133	1	1	1.796	2.209	
4B	4	2	1.727	1.899	1	2	-	-	Oval shape due to misplacement in fine grind
4C	4	3	1.690	1.800	1	3	1.797	2.169	
3A	3	1	1.755	2.057	6	1	1.799	2.198	
3B	3	2	1.726	1.919	6	2	1.794	2.150	
3C	3	3	1.686	2.269	6	3	1.792	2.678	
3D	3	4	1.651	2.160	6	4	1.798	2.512	
3E	3	5	1.617	2.335	6	5	1.789	2.815	

Table 1. Results of ultrasonic impact grinding of geodesic lenses. The depth measurement is in the unit of volts. (1.308 mV ≡ 1.0 μm) The designed lens depth is 1.797 V. Except sample 3E, the depth variations of all the samples after fine grind are within 0.3%.

diameter is 8.0 mm. Angular alignment of better than 10 sec can be achieved by optical means. We have used a tool maker square to check the perpendicularity before the grinding process is started. The angular accuracy obtained is better than 0.1°. To compensate for the slight angular misalignment, each lens was ground deeper into the substrate than the designed depth. Subsequently, the top flat surface was re-established using the lens axis as the reference. The whole substrate was tilted with respect to the polishing pad such that the polished flat surface touched the edge of the depression simultaneously. This compensation technique worked well for substrates having only one lens. We plan to incorporate an optical instrument into the new ultrasonic machine so that the angular requirements are met before grinding.

(4) The technique of ultrasonic impact grinding is proved to be precise, fast and economic. Reproducible results can be fairly easily obtained. The tool wear problem can be neglected if more than two tools are used for grinding the lens. Reference to Table 1 reveals that the five samples fine ground with tool tip No. 6 have resulting lens depressions with depth variation within 10 mW ($\sim$7.5 μm). The consistency of these lens depressions will be better than 7.5 μm if a third tool tip is used.

The Raytheon ultrasonic impact grinding machine is not designed for high precision work. We have to go through unnecessary steps to preserve the lens profile. Even with the great difficulties encountered, however, we were able to fabricate depressions within several μm of the designed profile. In order to meet the goal of precision machining, an upgraded impact grinding machine was purchased using internal funds. The new machine has the capability of controlling the depth within 1 μm. The preliminary test demonstrated a cutting speed about 50 times faster than the old machine. It took only 45 sec to grind a 1.4 mm deep, 8 mm diameter depression in $LiNbO_3$ substrate. The surface finish was also improved by reducing the tool strokes during the grinding of the last 25 μm.

(b) Diamond Turning and Diamond Generating

Task 1 of the statement of work of this contract involved an investigation of the use of numerically controlled precision machining for formation of geodesic lenses. Two techniques, single point diamond turning and diamond generating, were investigated.

Diamond turning is a precision cutting process using a single point diamond as the cutting edge to form the geodesic lens depression. Diamond turning machines are commercially available from Moore Special Tool Co. for fabricating aspherical optics. The major utility of this technique is for low cost, high precision infrared optics where tool marks on the surface can be tolerated. At these wavelengths, the machined surfaces are readily usable without additional polishing. When a $LiNbO_3$ single crystal is turned, the surface shows a hazy appearance in areas termed as unfavorable crystalline regions resulting from anisotropic crystalline properties. A delicate optical polish after turning is therefore necessary for fabricating integrated optic devices. This observation agreed with our experimental results, 5 μm peak-to-valley surface roughness was measured in the unfavorable regions of a flat diamond turned $LiNbO_3$ substrate.

Although the state-of-the-art diamond turning machines have a 1/4 μm control accuracy in both translational and rotational movements, the resulting lens profiles on $LiNbO_3$ have depth variation of up to 4.0 μm and the profile tolerance of about 3.0 μm. The poor depth control is attributed to troubles of gauging the depth and can be improved. However, the problem of profile tolerance of 3.0 μm is due to the fact that a large tool pressure is required to cut $LiNbO_3$ substrates. This is an intrinsic problem associated with the anisotropic characteristics of the material.

Diamond generating employs a diamond impregnated tool to grind the surface depression. The grinding is controlled by precision slides and spindles which are interfaced with a computer. This technique has been employed successfully to fabricate large diameter aspherical lenses (3-dimensional bulky lens). Special tools need to be developed for small radius aspherical shapes. A directed subcontract for diamond generating of 4 f/1.5 geodesic lenses in $LiNbO_3$ substrate has been given to a local optical shop, OPTI Systems, Inc. The profile tolerances of

the lenses are specified at 1/2 μm for two samples and 1 μm for the other two samples. The experimental results from OPTI Systems indicated that the surface damage due to diamond grinding was worse than expected, pieces of $LiNbO_3$ larger than the diamond grit size chipped off the surface during grinding. The depth of this subsurface damage varied from 6 to 10 μm peak-to-valley. We conclude that diamond generating is not an adequate technique for fabricating aspherical depressions in $LiNbO_3$ crystals.

SECTION IV

FABRICATION AND EVALUATION OF GEODESIC WAVEGUIDE LENSES

Three $LiNbO_3$ samples, 3A, 4A, and 4C, were polished during the second quarter of this program. The task of maintaining the lens profile during optical polish was a success. We have measured a depth change less than 1.0 μm after polish for all three samples. Optical waveguides were fabricated on these samples in a conventional way. Single mode waveguides were formed by diffusing 200 Å E-beam evaporated Ti at 1000°C. The diffusion time was 5 hours. Although the He-Ne laser light could propagate in the planar waveguide region, all the guided light terminated right at the lens edge. We had tried to add 200 Å more Ti onto samples 4A and 3C and repeated the diffusion process. Deeper waveguides and larger index change, however, did not eliminate the radiation problem. We believe the radiation is due to a sharp corner at the edge caused by the polishing of the top surface. Since there was no depth control in the Raytheon machine, we ground the depression all the way into the substrate. The overground portion was then removed by removing the top flat surface. Using the new machine we should be able to control the grinding process with high precision, thus eliminating the process of surface removal.

Since contract funds were not sufficient to grind and polish more geodesic lenses using the high precision ultrasonic impact grinding machine which was installed and operational in early February of 1979 we decided, with the approval from NRL (Naval Research Laboratory), to reprocess sample 3A, 4A and 4C. The Ti diffused waveguide layer was removed and the edges of the lens depressions were ground and repolished. The sharp corner at the lens edge was removed to ensure continuous propagation of waveguided light. As expected, the resulting lens profile was slightly deviated from the original designed one. Sample 4A was delivered to NRL at the end of this program.

The optical waveguide was formed on sample 4A by diffusing 300Å Ti into the $LiNbO_3$ substrate in an oxygen atmosphere. The diffusion temperature was 1000°C and the diffusion time was 6 h. Before diffusion, the Ti metal was oxidized at 600°C for 4 h. The waveguide can support two TE and two TM polarization modes. However, only the lowest order mode can propagate through

the lens depression. At GaAℓAs laser wavelength, the waveguide becomes single mode. For convenience, an He-Ne laser was used as the light source in the experiment. The focal length of the geodesic lens was determined by the deflection angle of the He-Ne laser light coupled out by a rutile prism positioned after the lens. The deflection angle was measured from the beam displacement and the distance between the lens and the detector. To reduce the effect of prism aberration on the measurement, the prism was positioned such that the focal point is approximated at the hypotenuse face of the prism.

Fig. 8 shows the measured focal length normalized to the radius of the depression as a function of the lateral displacement of the input beam. The focal length remains fairly constant over 85% of the lens depression the designed useful aperture. The slight tendency for the focal length to become shorter as the light beam moves away from the center of the lens could be due to either the profile deviation caused by the additional polishing mentioned previously, or the experimental inaccuracy.

The intensity distribution near the focal plane was measured using an expanded He-Ne laser beam. The rutile prisms were used to couple the laser light into and out of the waveguide. After the output prism, a relay lens (10x microscope objective with NA = 0.30) imaged and magnified the focal spot to a 7 - μm slit in front of the detector. New rutile prisms with 60° base angle were used in the experiment. As a result, a higher power microscope objective with short working distance can be utilized to reimage the focal plane. An iris at the input end controlled the width of the input beam. Fig. 9 shows the intensity distribution when the full aperture was illuminated. The 3dB spot size was 1.6 μm as compared to the theoretical spot size of 0.32 μm. The discrepancy is the result of the following three effects: (1) the resolution of a perfect 10x microscope objective is 0.93 μm (2) the presence of prism coupler introduces aberration (3) the deviation of lens profile from the ideal profile. Nevertheless, the spot size is the smallest ever measured. The side lobes to the right of the main peak could be due to severe in-plane scattering or lens aberration. When the relay lens was moved by a small amount in the longitudinal direction, the intensity distribution shown in Fig.10 was obtained. At this position the spot size is bigger (3dB width 2.5 μm), however, the side lobes in Fig.10 become diffused.

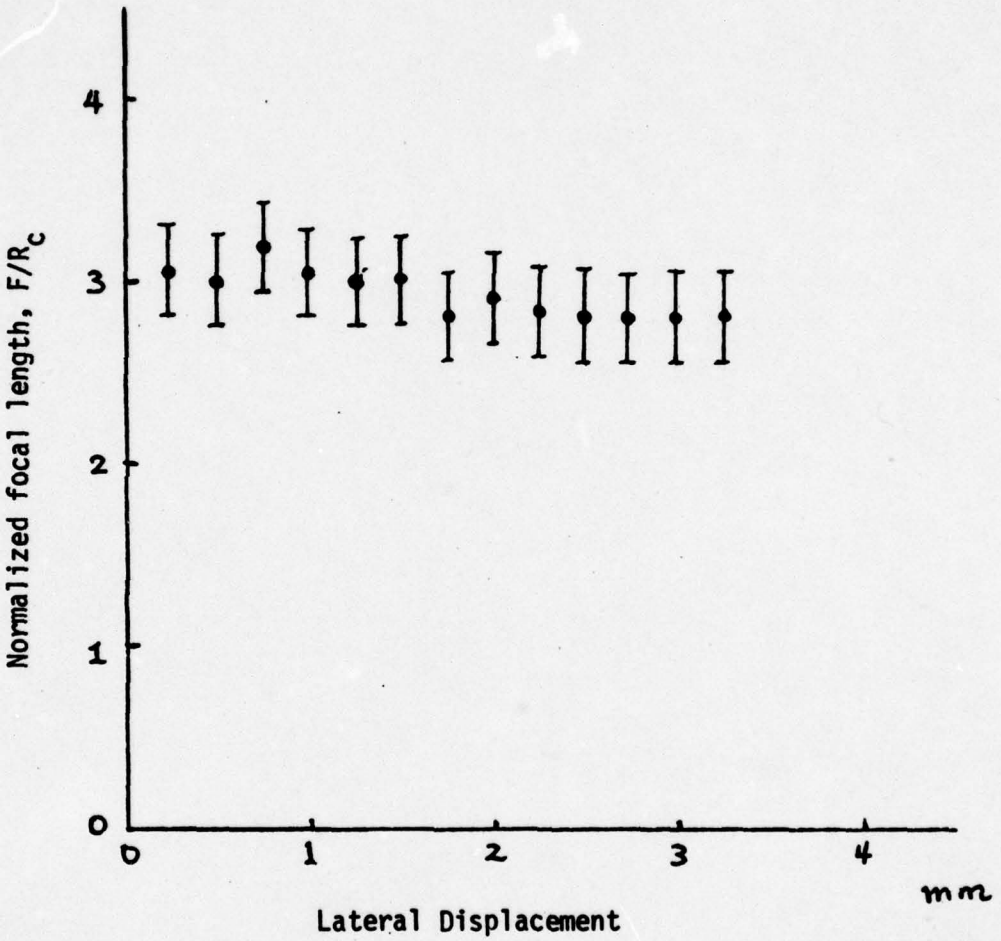

Fig. 8 Measured focal distance vs. lateral displacement of incident beam for geodesic lens fabricated in Ti:$LiNbO_3$ waveguide.

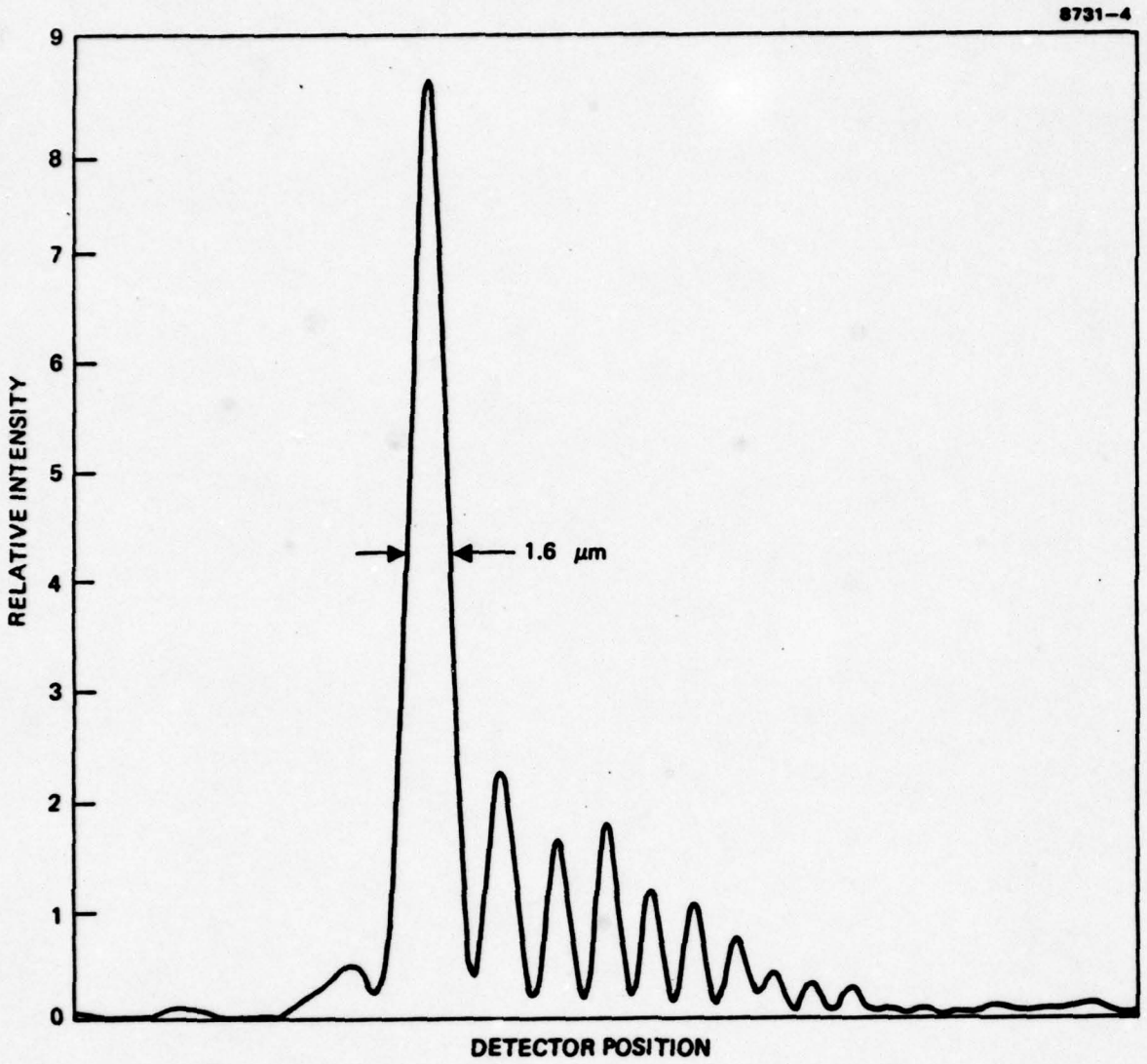

Fig. 9 Intensity distributed at the focal point for the geodesic lens fabricated in a Ti:$LiNbO_3$ waveguide.

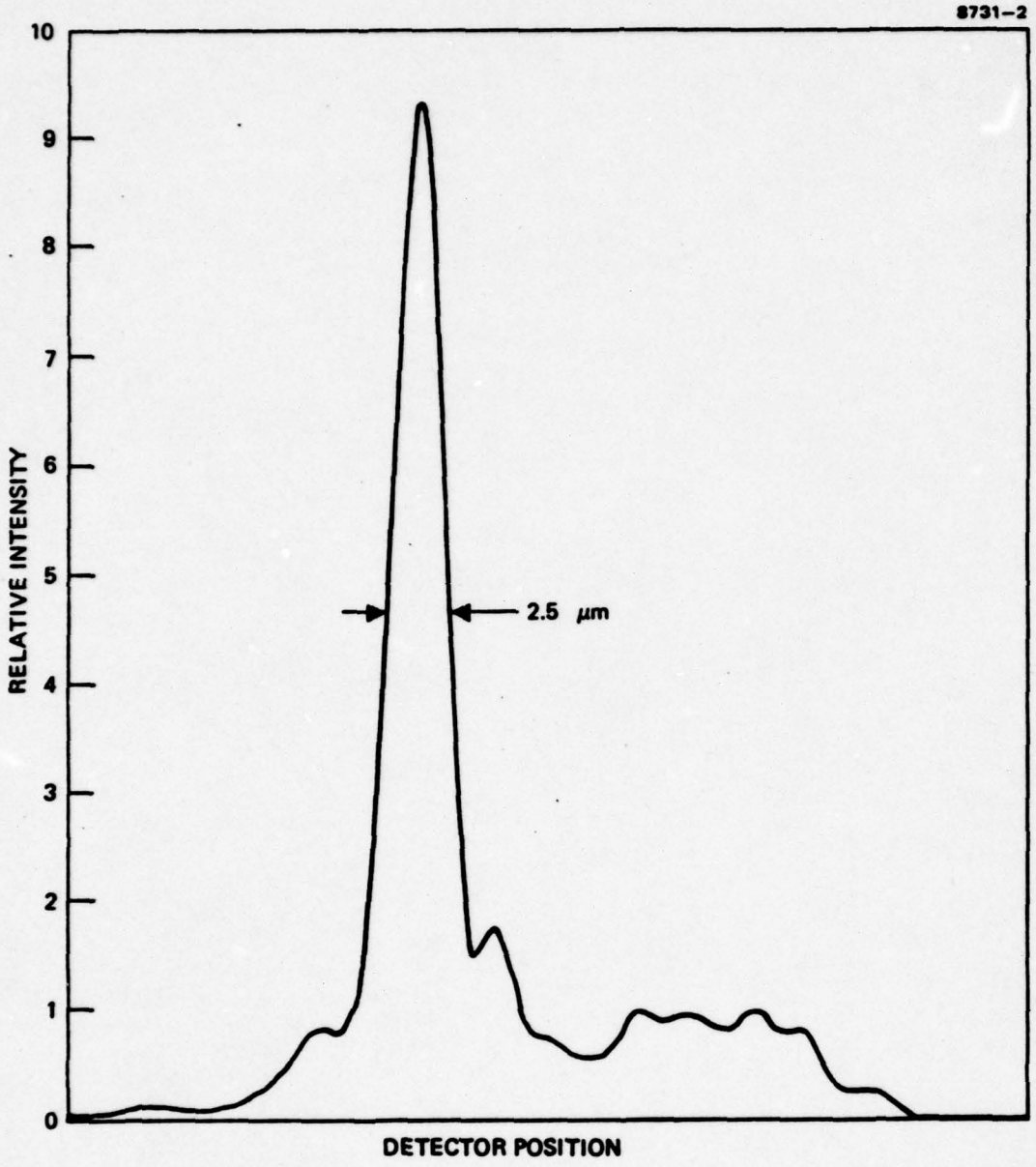

Fig.10 Intensity distribution near the focal point for the geodesic lens. The relay lens (microscope objective) was placed at a position where side lobe levels are lower.

SECTION V

COMPUTER ERROR ANALYSIS

(a) Ray Tracing Theory

In this section we summarize a ray-tracing technique for tracing rays on a rotationally symmetric geodesic lens. By Fermat's principle it can be shown that light rays travel along geodesic lines. The differential equations that the geodesics of a surface of revolution satisfy are:

$$\frac{d^2\theta}{ds^2} + \frac{2}{\rho}\frac{d\theta}{ds}\frac{d\rho}{ds} = 0 \tag{10}$$

$$\frac{d^2\rho}{ds^2} + \frac{g'g''}{1+(g')^2}\left(\frac{d\rho}{ds}\right)^2 - \frac{\rho}{1+(g')^2}\left(\frac{d\theta}{ds}\right)^2 = 0 \tag{11}$$

where θ is the angle of rotation, ρ is the distance from the axis of rotation, s is the path length traveled by the light ray inside the surface, and $g(\rho)$ is the function that describes the profile which generates the surface of revolution. g' and g" are the derivatives of $g(\rho)$ with respect to ρ. The differential equations given by (10) and (11) can be solved by separation of variables and rewriting the equations in the form of first-order linear differential equations. In a cylindrical coordinate system the solutions of the first order differential equations are reduced to

$$\theta(\rho) = \theta_0 = c \int_{\rho_0}^{\rho} \left(\frac{1+(g')^2}{\rho^2 - c^2}\right)^{1/2} \frac{d\rho}{\rho} \tag{12}$$

$$s(\rho) = \int_{\rho_0}^{\rho} \left(\frac{1+(g')^2}{\rho^2 - c^2}\right)^{1/2} \rho \, d\rho \tag{13}$$

where θ_0 is the initial azimuth of the entering light ray, ρ_0 is the outer radius of the lens, $c = \rho_0 \sin\theta_0$, and g' is the derivative of the profile with respect to the radius ρ of the cylindrical coordinate system. $\theta(\rho)$ is the azimuth and $s(\rho)$ is the path length of the ray measured from the point of entrance into the geodesic lens.

The ultimate goal of this task is to write a computer program for tracing rays through rotationally symmetric depression lenses. In order to determine the propagation direction of the light the tangent vector of the path was calculated. In a rectangular coordinate system the unit tangent vector, $\vec{t}$, is given by:

$$\vec{t}_{(\rho,\theta)} = \left[\frac{-\cos\theta}{\rho}\left(\frac{\rho^2 - c^2}{1 + (g')^2}\right)^{1/2} - \frac{c \sin\theta}{\rho}\right]\vec{e}_1 +$$

$$\left[\frac{-\sin\theta}{\rho}\left(\frac{\rho^2 - c^2}{1 + (g')^2}\right)^{1/2} + \frac{c \cos\theta}{\rho}\right]\vec{e}_2 +$$

$$\left[-\frac{g'}{\rho}\left(\frac{\rho^2 - c^2}{(1 + (g')^2}\right)^{1/2}\right]\vec{e}_3 \qquad (14)$$

where $\vec{e}_i$s are unit vectors along the i^{th} axis. The path of a light ray on the rotationally symmetric lens is symmetric, such that ρ (the radius used as a parameter to describe the path) decreases to a minimum of $\rho_o \sin\theta_o$ and then increases back to ρ_o. Thus the azimuth, θ_e, of the point where the light ray departs from the lens is:

$$\theta_e = \theta_o + \left|2c \int_{\rho_o}^{\rho_o \sin\theta_o} \left(\frac{1 + (g')^2}{\rho^2 - c^2}\right)^{1/2} \frac{d\rho}{\rho}\right| \qquad (15)$$

Substitute ρ_o, θ_e for ρ,θ in the equation of the tangent vector, Eq. (5) then $\vec{t}(\rho_o,\theta_e)$defines the direction of the outcoming ray. This in turn determines the "focal distance", f, of the ray. f is defined as the distance between the lens center and the point where the outcoming ray crosses the lens axis and can be expressed in the simple form

$$f = \left|\frac{\rho_o \sin\theta_o}{\sin(\theta_o + \theta_e)}\right| \qquad (16)$$

The total optical path length of the ray is

$$s_e = s_o + 2\left|\int_{\rho_o}^{\rho_o \sin\theta_o} \left(\frac{1 + (g')^2}{\rho^2 - c^2}\right)^{1/2} \rho\, d\rho\right| \qquad (17)$$

The ray-tracing technique summarized above was checked on results which are proven correct. Two special uses of the above equations will be outlined below. Their application to lens tolerance analysis will be pointed out.

First example is the investigation of the focusing properties of spherical depressions. For spherical depressions

$$\theta_e = \theta_o + \left|\frac{\pi}{2} - \arcsin\left(\frac{\rho_o^2 \sin^2\theta_o + (1-2\sin^2\theta_o)R^2}{\rho_o^2 \sin^2\theta_o - R^2}\right)\right| \qquad (18)$$

and for the limiting case of paraxial ray

$$\lim_{\theta_o \to 0}\left(\frac{f}{\rho_o}\right) = \frac{1}{2(1-\cos\psi)} = \frac{R}{2(R - \sqrt{R^2 - \rho_o^2})} \qquad (19)$$

where ψ is the polar angle and R is the radius of the sphere, a portion of which creates the depression. This agrees with published results for spherical depressions.

In tolerance analysis of geodesic lenses this example of spherical depression is useful, since the explicit and relatively simple equation for the focal length allows one to estimate changes in the focal length of geodesic lenses resulting from slight deviations in the shape and depth of the lens.

Another example for rotationally symmetric surfaces is a toroidal section ($g(\rho) = r - \sqrt{r^2 - (\rho_o - \rho)^2}$) generated by the section of a circle of radius r. The importance of this surface of rotation is that it can be viewed as a rounding to the lens, and in that sense it is a prototype of any kind of rounding. To know the focusing behavior of such surfaces is important in the construction of rounded edge geodesic lenses. In fact, when a particular focal length is desired in connection with circular rounding the question is whether any light beam parallel to the central ray when entering the toroidal section will terminate its path in the direction of the desired focal point. The solution of this problem involves elliptical integrals of the first, $F(\lambda, q)$, and third, $\pi(\lambda, n, q)$, kinds.

$$\theta_e = \theta_o + |A\,F(\lambda, q) + B\,\pi(\lambda, n, q)| \qquad (20)$$

where

$$A = \frac{\sqrt{4r\rho_o \sin\theta_o}}{\rho_o - r}, \qquad B = A\left(\frac{\rho_o - r}{\rho_o \sin\theta_o} - 1\right),$$

$$\lambda = \sin^{-1}\left(\frac{\rho_0(1-\sin\theta_0)}{r+\rho_0(1-\sin\theta_0)}\right)^{1/2}, \qquad n = \frac{(\rho_0-r)(r+\rho_0(1-\sin\theta_0))}{2r\,\rho_0\,\sin\theta_0}$$

$$q = \frac{[r+\rho_0(1-\sin\theta_0)][\rho_0(1+\sin\theta_0)-r]}{4\,\rho_0\,r\,\sin\theta_0}$$

The focal distance for each ray which path stays entirely on the toroidal rounding section is then given by equation (7). These equations can be applied to determine the effects of variation in the lens rounding.

(b) Computer Program

A ray trace program has been developed using Eqns. (14)-(17). This was not a trivial task in that the available integration routines were not adequately accurate. This was due to the fact that the integrand contains at least one singularity and in some cases two. In addition the normal technique of integration by parts to eliminate a singularity of this form did not work because the test case profile has a discontinuous $g''(\rho)$. This test case profile defines an aberration-free lens with focal point on the lens edge.

An algorithm for calculating the integral has been found and included in our computer library. This algorithm uses the orthogonality properties of the Chekyshev polynomials. The development is analogous to that followed in producing the Gauss-Legendre and Gauss-Laguerre quadratures. In this case, the pertinent integral and corresponding Gauss-Chekyshev quadrature formula are given by

$$\int_{-1}^{1} \frac{1}{\sqrt{1-z^2}}\,F(z)\,dz = \sum_{i=0}^{n} \omega_i\,F(z_i)$$

The integration is exact if $F(z)$ is a polynomial of degree $2n+1$ or less. Note the singularity at $z = \pm 1$. The focal position for a fan of input rays is given in Table 1 . These data are for an F/1.5 lens. The heights and focal positions are normalized to the lens radius of 1.

Table 1

Input Height	Focal Position
.00684	.99962
.04496	.99977
.11466	.00002
.16573	.99999
.21358	.99996
.25728	.99996
.29596	1.00001

Previous results using Simpson rule and Gauss-Legendre quadratures were at best accurate to two figures. In some cases the results were off by factors of 2 or 3. Presently we can trace rays through a geodesic lens with at least four figure accuracy. This is felt to be adequate for purposes of further tolerance analysis, system design and evaluation of IOSA concepts. This program does not require the equivalent lens transformation.

It is also possible to design lenses by combining this new capability with existing optimization routines. One method for doing this is to:

(1) Define several points on an initial profile

(2) Fit a cubic spline curve through these points. (This curve has zero slope at the edge and center of lens.)

(3) Use optimization routines to determine profile by varying the depth at the initial points. This final step requires ray tracing.

(c) Tolerance Analysis

Eq. 15 provides a very convenient way of performing tolerance analysis of a geodesic lens design. Given the profile and the variation of interest, the slope at each point in the lens can be determined. In a focal system such as shown in Figure 11, the separation between a ray and the optical axis for any distance from the lens center, f, is given by

$$d = R \sin \theta_e + (f + R \cos \theta_e)\tan (\theta_o + \theta_e) \qquad (21)$$

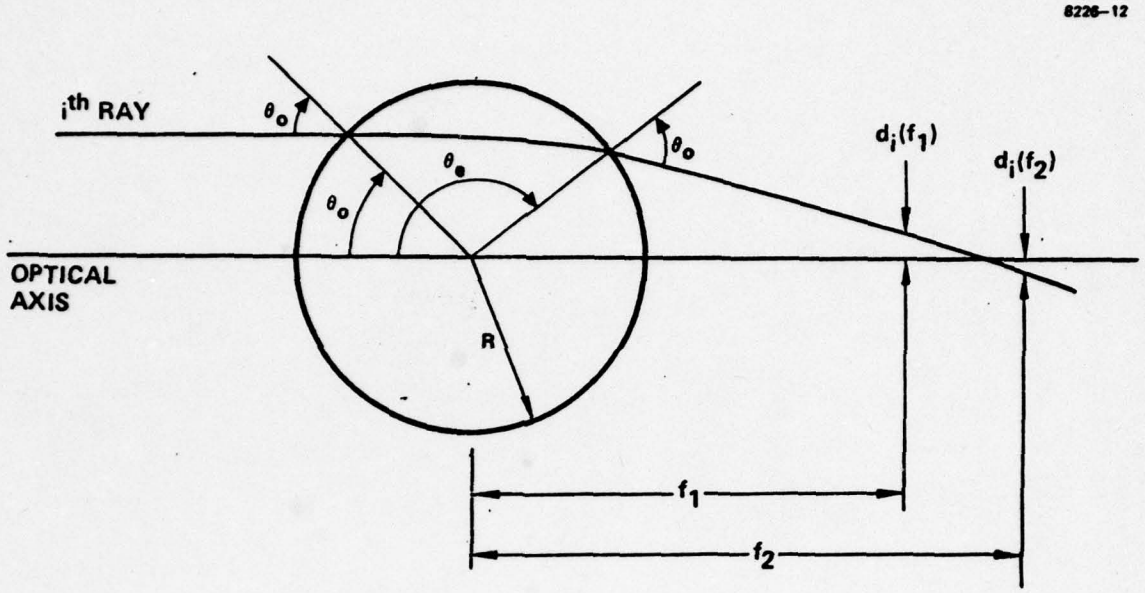

Fig.11 Focal optical system showing parameters used in the calculation of the geometrical spot size. The focal length is defined as the length f where $\sqrt{\sum_i (d_i(f))^2}$ is a minimum. The spot size is the full extent of the rays at this point.

The distance from the center of the lens to the ray intersection with the optical axis is given by

$$F = \left| \frac{R \sin \theta_o}{\sin(\theta_o + \theta_e)} \right| \qquad (22)$$

For a lens that does not conform to the optimum profile, F is a function of the ray; hence, the focal position for the tolerance analysis was chosen as the position, f_m, of minimum

$$D(f) = \sqrt{\sum_i d_i(f)^2} \quad , \qquad (23)$$

where $d_i(f)$ is the distance of the i^{th} ray from the optical axis at a distance f from the center of the lens. Figure 11 illustrates these parameters. The minimum is found by numerically searching for the minimum by varying the distance f between the extremes in the focal position of the individual rays.

Two functional variations from the optimum profile have been analyzed. In the first, the lens depth was varied by

$$\Delta y/y = \text{constant}, \qquad (24)$$

where Δy is the variation, and y is the initial depth. Both Δy and y are functions of the radial position, ρ. This particular variation represents an error caused by tool wear during impact grinding. In the second variation a percentage of the upper portion of the lens was neglected while the profile was maintained. Experimentally, this corresponds to either not grinding deep enough or to polishing away a portion of the lens rounding.

The profile of an f/1.5 lens was used in the calculations; some results are given in Figs. 12 through 14. Figure 12 shows the increase in focal length versus the percentage decrease in depth for tool wear and for surface removal. For each unit decrease in total depth for tool wear, there is approximately a 13 unit change in focal length. With surface removal, the change in focal length is about 3 units per unit change in depth.

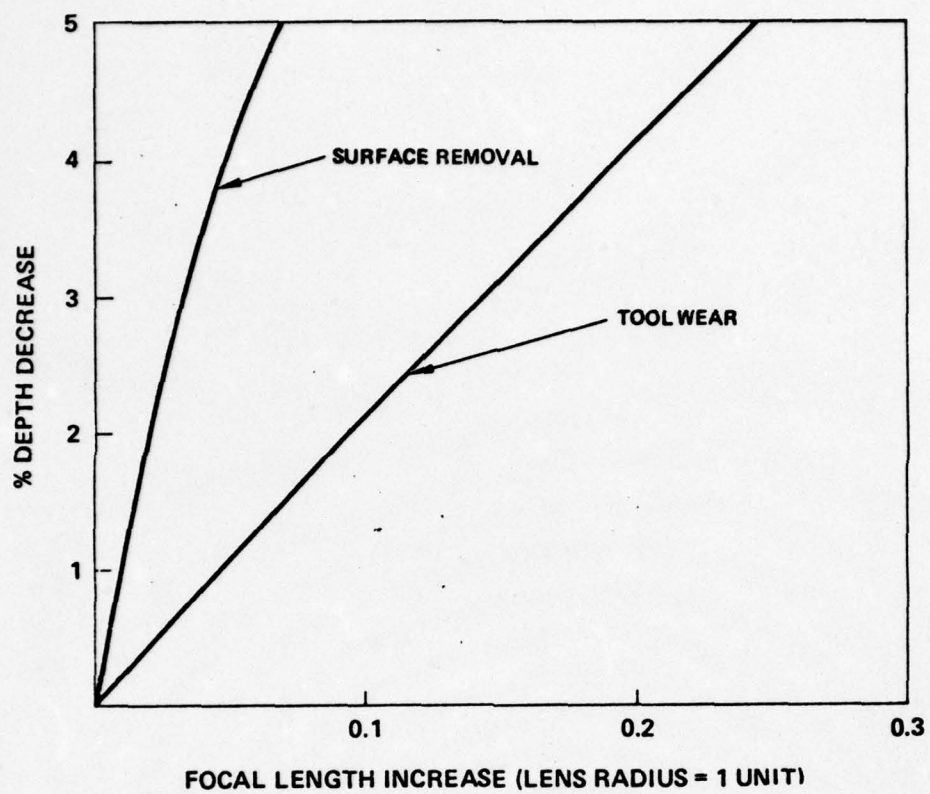

Fig.12 Focal length increase vs % of depth decrease for both tool wear and surface removal.

A spot diagram at the focal position for 100 rays and a 2% tool wear depth change is shown in Figure 14. The most interesting thing about this diagram is the tight core and the few scattered rays outside of this core. These scattered rays are those passing through approximately the outer 10% of the original useful aperture. Another point of interest is that all the spot diagrams provided have this feature of a tighter core for 90% of the useful aperture. This is further illustrated in Figure 14, where the geometrical spot sizes for full aperture and for 90% aperture are plotted versus the % depth decrease.

For an f/1.5 lens in $LiNbO_3$, the full lobe width of a Gaussian beam truncated at the 1/e point is $\sim$1.4 μm at a free space wavelength of 0.8 μm. For a 1-cm-diameter lens, this corresponds to 3×10^{-4} units in Figure 15. Hence, to maintain diffraction limited performance, a depth change of 1% can be tolerated if 90% of the original useful aperture is utilized. For even worse tool wear, a smaller aperture is required to maintain diffraction limited performance. (13)

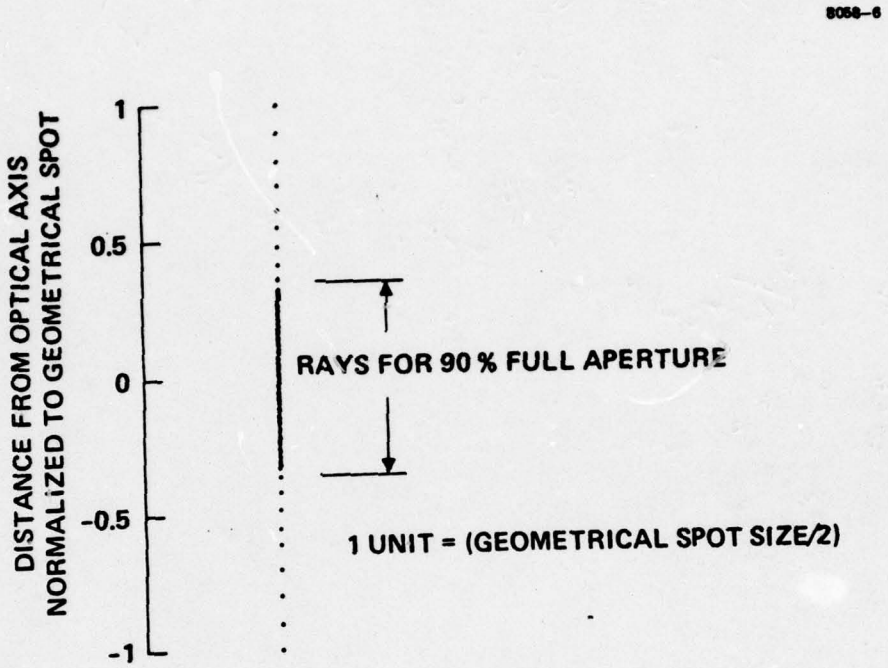

Fig. 13 Spot diagram for a 2.0% total tool wear depth decrease.

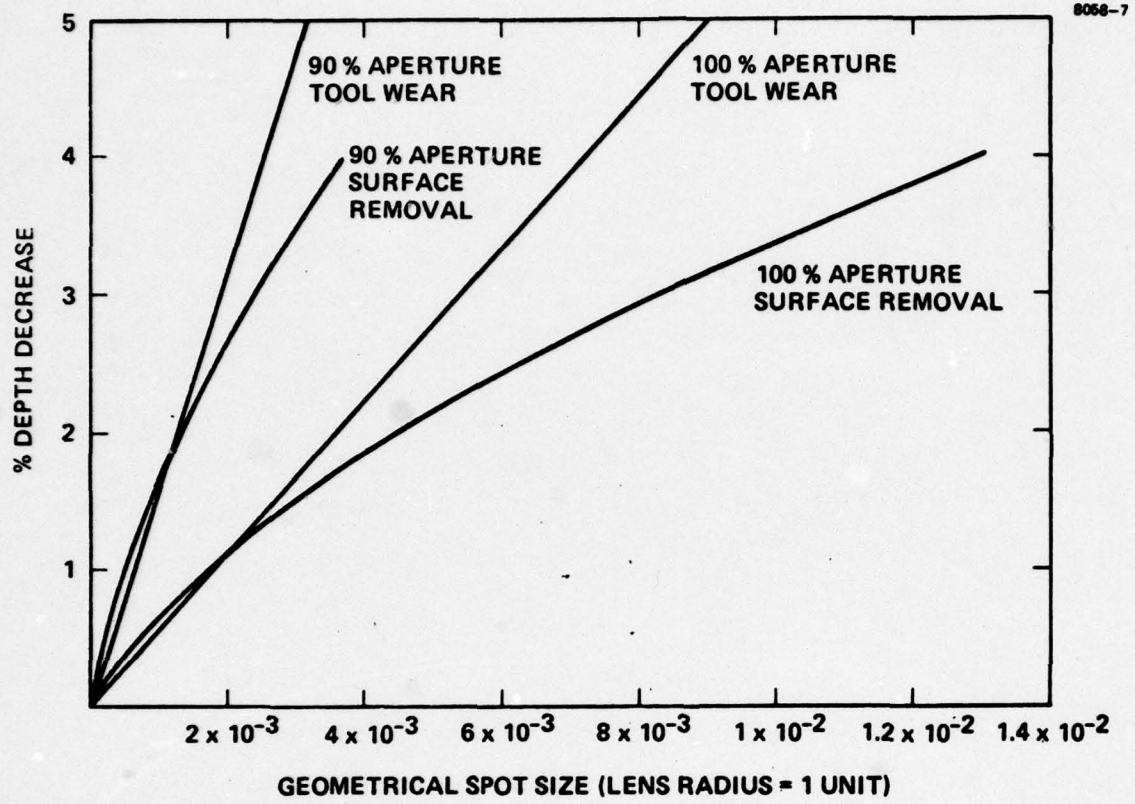

Fig.14 Geometrical spot size vs % of depth decrease for both tool wear and surface removal. Two curves are provided for each one corresponding to 100% and 90% of the original useful aperture.

SECTION VI

CONCLUSIONS AND SUGGESTIONS

Under this program, we have successfully developed the ultrasonic impact grinding technique for the fabrication of aspherical geodesic lens depressions. The lens radius is 4 mm and the depth is 1.374 mm. 15% of the lens aperture is allocated for a curved rounding at the edge of the depression. The designed focal length is 10.2 mm for an aberration free aperture of 6.8 mm, thus the f number of the lens is 1.5. The technique of ultrasonic impact grinding is proved to be precise, fast and economic. Reproducible results can be easily obtained. The tool wear problem can be neglected if more than two tools are used for grinding the lens. We have demonstrated that depth variation within 7.5 μm for 5 depressions can be obtained using two tools. One of the 5 depressions has the exact designed depth. The consistency of the lens depressions can be further improved if a third tool is used. The grinding process is fast using the 200 W Bullen machine. It takes only 45 sec. to grind a 1.4 mm deep, 8 mm diameter depression in $LiNbO_3$ substrate. The machine is easy to operate once the optimum grinding parameters are set.

Aberration free geodesic lenses have been fabricated in $Ti:LiNbO_3$ waveguides. The measured focal length is fairly close to the designed 10.2 mm even though the lens profile is slightly off the ideal profile. The major problem encountered is the polishing of the lenses. There are many fine scratches at the edge of the depression, causing excessive propagation loss and in-plane scattering. The measured 3dB focal spot size is 1.6 μm as compared to the theoretical value of 0.32 μm. The discrepancy is believed to be the sum of the following three effects. (1) The resolution of a perfect 10x microscope objective with NA = 0.3 is 0.93 μm. (2) The use of prism coupler to extract guided light out of waveguide causes aberration. The rutile prism is uniaxial and will introduce additional aberration. (3) The actual lens profile is slightly off the ideal designed profile. More sophisticated measurement technique has to be developed to evaluate small f number lens with submicron focal spot size. The polishing process also has to be improved, otherwise, the in-plane scattering due to scratches will

bury the side lobe information and limit the useful dynamic range of the lens system. It is important to emphasize that the polishing process should not destroy the lens profile.

An extensive computer error analysis is completed under the program. The purpose of this study is to determine the effect of deviation of the actual profile from the ideal profile on the spot size and focal length. A ray tracing through geodesic lens depression is developed from which the geometric spot size and focal length are calculated. For an f/1.5 lens in $LiNbO_3$, the full lobe width of a Gaussian beam truncated at the 1/e points is about 1.4 μm assuming the free space wavelength is 0.8 μm. For a 1 cm diameter lens, a depth change of 1% can still maintain its diffraction limited performance if 90% of the original useful aperture is utilized. On the other hand, the focal length is very sensitive to the depth variation. We have shown that for each unit decrease in total depth for tool wear, there is approximately a 13 unit change in focal length. With surface removal, the change in focal length is about 3 units per unit change in depth. Unless one can control the depth better than 1.0 μm, the integration of geodesic lenses in integrated optic circuits is an extremely difficult job. At the current stage, in any optic system using geodesic lenses, the precise location (within several μm) of the focal plane will have to be determined after the lens is fabricated.

REFERENCES

1. M. C. Hamilton, D. A. Wille, and W. J. Miceli, "An integrated optical RF spectrum analyzer," in Proc. IEEE 1976 Ultrasonic SYmp. Annapolis, MD.

2. M. K. Barnoski, B. Chen, H. M. Gerard, E. Marom, O. G. Ramer, W. R. Smith, Jr., G. L. Tangonan, and R. D. Weglein, "Design, fabrication and integration of components for an integrated optics spectrum analyzer," in Proc. IEEE 1978 Ultrasonic Symp., Cherry Hill, NJ.

3. B Chen, E. Marom, and R. J. Morrison, "Diffraction limited geodesic lens for integrated optics circuits," Appl. Phys. Lett. vol. 33, pp. 511-513, Sept. 1978, and references therein.
The most recent reference on geodesic lens is by G. C. Righini, V. Russo, and S. Sottini, "A family of perfect aspherical lenses for integrated optical circuits," IEEE J. Quant. Elect., vol. QE-15, pp. 1-3, 1979.

4. P. R. Ashley and W.S.C. Chang, "Fresnel lens in a thin-film waveguide," Appl. Phys. Lett. vol. 33, pp. 490-492, Sept. 1978.

5. S. K. Yao and D. B. Anderson, "Shadow sputtered diffraction-limited waveguide Luneburg lenses," Appl. Phys. Lett. vol. 33, pp. 307-309, Aug. 1978.

6. S. K. Yao and D. E. Thompson, "Chirp-grating lens for guided-wave optics," Appl. Phys. Lett., vol. 33, pp. 635-637, Oct. 1978.

7. Gen-ichi Hatakoshi and Shun-ichi Tanaka, "Grating lenses for integrated optics," Opt. Lett. Vol. 2, pp. 142-144, June 1978.

8. P. K. Tien, "Method of forming novel curved-line gratings and their use as reflectors and resonators in integrated optics," Opt. Lett. Vol. 1, pp. 64-66, Aug. 1977.

9. D. Kassai and E. Marom, "Aberration-corrected rounded-edge geodesic lenses," to be published in J. Opt. Soc. Am.

10. M. Heiblum and J. H. Harris, IEEE J. Quant. Elect. QE-11, 75 (1975).

11. A. W. Snyder and J. D. Love, Opt. Comm. 12, 326 (1974).

12. H. G. Unger, Planar Optical Waveguides and Fibers, Clarendon Press, Oxford 1977.

13. E. Marom, B. Chen and O. G. Ramer, "Spot Size of Focused Truncated Gaussian Beams", Opt. Engin. Vol. 18, pp. 79-81, Jan/Feb 1979.